Medical Engineering & Physics 36 (2014) 800–804

Contents lists available at ScienceDirect

Medical Engineering & Physics

journal homepage: www.elsevier.com/locate/medengphy

Communication

New experimental protocols for tensile testing of abdominal aortic analogues

L. Bailly[a,*], V. Deplano[a], A. Lemercier[a,b,c,d], O. Boiron[a], C. Meyer[a]

[a] Aix Marseille Université, CNRS, Centrale Marseille, IRPHE UMR 7342, 13384 Marseille, France
[b] Univ. Grenoble Alpes, 3SR, F-38000 Grenoble, France
[c] CNRS, 3SR, F-38000 Grenoble, France
[d] MDB Texinov, 38354, La Tour du Pin, France

ARTICLE INFO

Article history:
Received 24 July 2013
Received in revised form
17 December 2013
Accepted 6 February 2014

Keywords:
Arterial analogue
Porcine aortic tissue
Uniaxial tensile tests
Physiological loadings
Elongation rates
Experimental protocols

ABSTRACT

This work proposes an *in vitro* tensile testing protocol that is able to characterize abdominal aortic (AA) analogues under physiologically inspired mechanical loadings. Kinematic parameters are defined in agreement with *in vivo* measurements of aortic dynamics. A specific focus is given to the choice of the applied loading rates, deriving from the knowledge of aortic Peterson modulus and blood pressure variations from diastolic to systolic instants. The influence of physiological elongation rates has been tested on both porcine AAs and a thermoplastic polyurethane (TPU) material used to elaborate AA analogues. The diastolic and systolic elongation rates estimates vary between orders of magnitude $\mathcal{O}(10^{-2})$ and $\mathcal{O}(10^{-1})\,s^{-1}$. Negligible differences are obtained when comparing stress–elongation responses between both physiological elongation rates. In contrast, a noticeable stiffening of the TPU mechanical response is observed compared to that obtained under the common low traction rate of $\mathcal{O}(10^{-3})\,s^{-1}$. This work shows how relevant physiological elongation rates can be evaluated as a function of age, gender and pathological context.

1. Introduction

Abdominal aortic aneurysm (AAA) is a permanent dilatation of the abdominal aorta (AA). Fundamental knowledge of AAAs dysfunctional biomechanics requires the mechanical characterization of aortic tissue under appropriate (patho-)physiological conditions. Alternatively to *in vivo* investigation of vascular mechanics, deformable AAA analogues have been made in the last decades. Most were placed into vascular flow simulators to investigate endovascular aneurysm repair [1–4] or fluid–structure interactions within AAAs [5,6]. Inflation testing was also conducted to identify AAAs deformation [7,8]. Yet, the intrinsic material properties of AAA analogues have been barely investigated and when they were [9,10], the testing kinematic conditions were not discussed in connection with previous protocols carried out on biological samples.

Numerous *in vitro* tensile tests have been reported to determine the mechanical behaviour of human AA/AAA [11–16] and porcine AA [17–20]. The typical protocol begins with a preconditioning phase (5–10 cycles) applied at a peak strain (5–10%) and constant elongation rate ($10^{-3}\,s^{-1}$), followed by a monotonic stretching to a chosen peak strain. Such measurements showed AA hyperelastic and anisotropic mechanical behaviour. Aortic wall's nonlinear viscoelastic properties were also demonstrated, albeit by very few studies [21,18,20]. Therefore, two factors are commonly discarded in experimental protocols, which make them unsuitable for mimicking physiological mechanical loadings:

- A single elongation rate is often considered during the characterization. So, periodic changes of tissue elongation rate occurring during the cardiac cycle are neglected.
- The relevance of the chosen elongation rate magnitude has been barely discussed regarding to *in vivo* mechanical loadings [22].

This study aims to propose a tensile-testing protocol able to characterize aortic analogues under mechanical loadings closer to *in vivo* loadings using suitable elongation rates, to test the influence of these elongation rates on both porcine AAs, and a polymer used in a recent vascular flow simulator [23,5].

* Corresponding author. Tel. +33 4 13 55 20 27.
E-mail address: lucie.bailly@irphe.univ-mrs.fr (L. Bailly).

http://dx.doi.org/10.1016/j.medengphy.2014.02.005
1350-4533/

2. Materials and methods

2.1. Materials

2.1.1. Aortic analogue

An idealized AAA model was manufactured using a mixture of Estane® 5714 TPU [7]. Eight rectangular samples (S_i, $i \in [1...8]$) were cut from tubular sections along orthoradial $\boldsymbol{e}_\theta$ and longitudinal $\boldsymbol{e}_l$ directions. Unloaded original length l_0, width w_0 and thickness t_0 were measured (±0.01 mm). Undeformed cross-sectional area was derived as $S_0 = w_0 \times t_0$.

2.1.2. Biological tissue

Three healthy AA tubular samples were excised from three 4-month old male pigs weighing 31 ± 4 kg. Experimental procedure was approved by the ethics board of the Surgical Center for Education and Research at Marseille's Nord Hospital. Five rectangular strips (B_i, $i \in [1...5]$) were cut along $\boldsymbol{e}_l$. B_1 and B_2 (resp. B_4 and B_5) were extracted from the same aortic sample.

Strips' dimensions are summarized in Table 1.

2.2. Methods

S_i and B_i biomechanical behaviour was investigated using a uniaxial tensile-testing device [7]. The actual force f, and length l, in the stretch direction were measured. The corresponding Cauchy stress σ was calculated as the load f per unit of actual cross-section S. Prior to a kth test performed on a strip, initial length l_0^k and force f_0^k were measured (optional index $k = 0$ refers to the undeformed configuration, *e.g.* $l_0^0 = l_0$). These values could differ from l_0 and null tension, when a previous load yielded to a residual elongation $\lambda^k = l/l_0^k$ and non-zero pre-stress $\sigma_0^k = f_0^k l_0^k/(S_0 l_0)$. Elongation rate during test k refers to the absolute time derivative $|\dot{\lambda}^k|$.

2.2.1. Preliminary stretch failure tests

Failure tests were performed on B_1 and B_2 at $|\dot{\lambda}^0| = 10^{-3}\,\mathrm{s}^{-1}$, allowing comparison with published data on longitudinal porcine and human AA specimens. Fig. 1 shows the similar material properties of human AA wall and porcine tissue under test.

2.2.2. Physiologically inspired protocols

This part focuses on elaborating physiologically inspired protocols using more suitable kinematic parameters. According to above results, our approach was based on the human AA Peterson modulus value:

$$E_p = D_d \frac{P_s - P_d}{D_s - D_d}, \tag{1}$$

where P_s, P_d, D_s, D_d represent the systolic and diastolic pressure and diameter. Its *in vivo* evaluation derives from measurements of maximal luminal diameters and blood pressure variations from peak diastolic to systolic instants, referred as t_d and t_s [24,25]. Arterial cyclic motion occurs predominantly in the circumferential direction [26,27]. Therefore, assuming AA as an incompressible thin-walled cylindrical tube [12,25], AA tissue undergoes a periodic maximal elongation λ_m, assessed by:

$$\lambda_m = 1 + \frac{D_s - D_d}{D_d} = 1 + \frac{P_s - P_d}{E_p}, \tag{2}$$

Aortic tissue average elongation rates occurring during diastole and systole can be determined as $|\dot{\lambda}_d| = |\Delta\lambda|/\Delta t_d$ and $|\dot{\lambda}_s| = |\Delta\lambda|/\Delta t_s$, where $\Delta\lambda = \lambda_m - 1$ represents the maximal variation of tissue elongation between systolic and diastolic peaks, Δt_d, the diastole

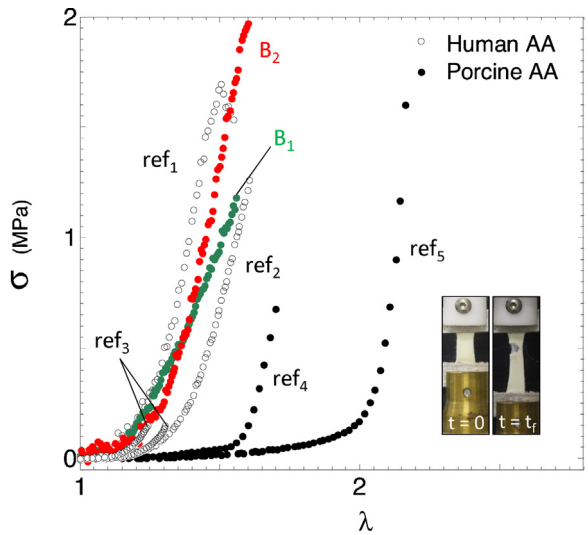

Fig. 1. Comparison between experimental data derived from monotonic tensile tests conducted on porcine and human AA specimens. Measurements of the present study carried out on porcine samples B_1 and B_2 are plotted in color, by contrast with previous data reported by [12] [ref$_1$], [16] [ref$_2$], [11] [ref$_3$], [20] [ref$_4$] and [17] [ref$_5$]. Pictures represent two typical configurations of a tested strip at initial ($t = 0$) and failure ($t = t_f$) shot-instants.

Table 1
Geometrical and initial load parameters of the synthetic and biological samples tested in the present uniaxial loading measurements. Indice k in l_0^k and f_0^k refers to test number k performed at a constant specific elongate rate $|\dot{\lambda}^k|$ ($k \in [1...3]$).

Sample	Axis	t_0 (mm)	w_0 (mm)	l_0 (mm)	$\alpha = l_0 : w_0$ (-)	l_0^1 (mm)	l_0^2 (mm)	l_0^3 (mm)	f_0^1 (N)	f_0^2 (N)	f_0^3 (N)
Synthetic AA											
S_1	$\boldsymbol{e}_l$	0.22	5	15	3.0	15.00	15.37	15.69	0.01	0.26	0.49
S_2	$\boldsymbol{e}_l$	0.26	5	15	3.0	15.50	15.91	16.21	0.01	0.25	0.48
S_3	$\boldsymbol{e}_l$	0.27	5	16	3.2	16.00	16.36	16.66	0.01	0.22	0.44
S_4	$\boldsymbol{e}_\theta$	0.22	5	15	3.0	15.00	15.40	15.76	0.01	0.27	0.52
S_5	$\boldsymbol{e}_\theta$	0.22	5	15	3.0	15.00	15.29	15.56	0.01	0.26	0.47
S_6	$\boldsymbol{e}_\theta$	0.23	5	16	3.2	16.00	16.43	16.75	0.01	0.27	0.46
S_7	$\boldsymbol{e}_l$	0.22	5	15	3.0	15.00	15.47	15.85	0.01	0.20	0.44
S_8	$\boldsymbol{e}_l$	0.28	5	16	3.2	16.00	16.31	16.85	0.01	0.26	0.45
Biological AA											
B_1	$\boldsymbol{e}_l$	1.30	9.90	19.40	1.9	–	–	–	0.02	–	-
B_2	$\boldsymbol{e}_l$	1.40	7.00	26.90	3.8	–	–	–	0.01	–	-
B_3	$\boldsymbol{e}_l$	1.49	5.66	15.52	2.7	22.38	22.73	26.10	0.01	0.02	0.08
B_4	$\boldsymbol{e}_l$	1.20	4.50	19.00	4.2	22.55	24.89	27.18	0.01	0.05	0.09
B_5	$\boldsymbol{e}_l$	1.10	8.00	21.50	2.7	25.03	27.43	29.71	0.09	0.16	0.16

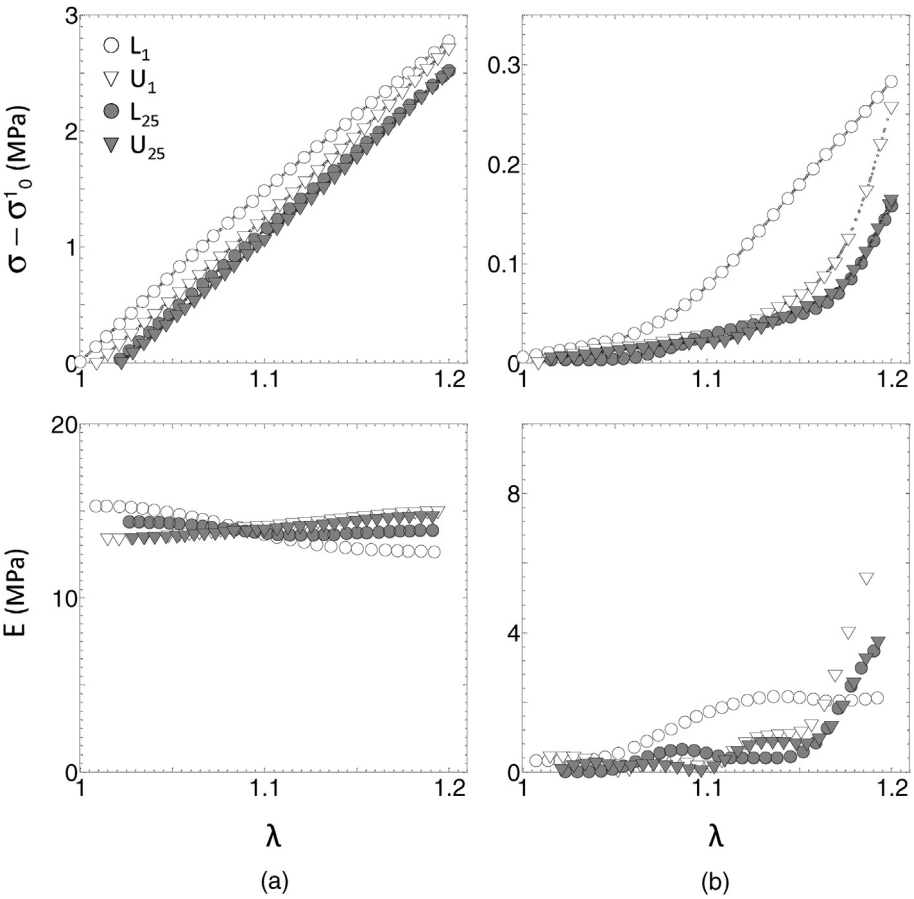

Fig. 2. **(a)** Comparison between experimental stress $\sigma - \sigma_0^1$ (*up*) and tangent modulus E (*bottom*), as a function of elongation λ during cycle 1 (comprising load L_1 and unload U_1) and cycle 25 (comprising load L_{25} and unload U_{25}) for synthetic sample S_5 tested at diastolic loading rate $|\dot{\lambda}_d|$ ($k = 1$); **(b)** Same as **(a)** in case of a typical biological sample (B_3).

duration and Δt_s, the systole duration. Values representative of healthy AA conditions ($P_s - P_d$ = 40 mmHg, E_p = 1.90 × 10^5 Pa, Δt_d = 0.73 s, Δt_s = 0.20 s) yield to $|\dot{\lambda}_d| \approx 4 \times 10^{-2}\ s^{-1}$ and $|\dot{\lambda}_s| \approx 1.5 \times 10^{-1}\ s^{-1}$.

S_i were subjected to three cyclic sequences at different elongation rates, noted $|\dot{\lambda}^1|$, $|\dot{\lambda}^2|$ and $|\dot{\lambda}^3|$ by order of application. The choice of the applied values directly derives from $|\dot{\lambda}_d|$, $|\dot{\lambda}_s|$ and a comparative value chosen by [12] to test human AA mechanical response, defined by $|\dot{\lambda}_c| = 1.4 \times 10^{-3}\ s^{-1}$. Finally:

- $\forall i \in [1 \ldots 6]$, S_i were tested using $|\dot{\lambda}^1| = |\dot{\lambda}_d|$, $|\dot{\lambda}^2| = |\dot{\lambda}_s|$ and $|\dot{\lambda}^3| = |\dot{\lambda}_c|$;
- S_7 was tested so that $|\dot{\lambda}^1| = |\dot{\lambda}_c|$, $|\dot{\lambda}^2| = |\dot{\lambda}_d|$ and $|\dot{\lambda}^3| = |\dot{\lambda}_s|$;
- S_8 was tested so that $|\dot{\lambda}^1| = |\dot{\lambda}_s|$, $|\dot{\lambda}^2| = |\dot{\lambda}_c|$ and $|\dot{\lambda}^3| = |\dot{\lambda}_d|$.

Each sequence comprised 25 load/unload cycles limited by a peak elongation of 1.20 [15]. Characteristic decay length being of the order of the strip's width for homogeneous isotropic materials [33,34], the central third of the strip's total dimensions was considered free from edge effects due to gripping constraints. Two ink 5 mm-spaced markers were drawn on this central region in order to allow optical recording of local elongation fields during measurements using a CCD camera (300 × 576 pixels, spatial resolution 0.11 mm/pixel) (results not shown). Due to the limited availability of tissue, B_3, B_4 and B_5 were solely subjected to one cyclic sequence at diastolic rate $|\dot{\lambda}_d|$.

3. Results

3.1. Mechanical response at $|\dot{\lambda}_d|$

S_i and B_i mechanical behaviours were investigated in response to the first sequence ($k = 1$), achieved at $|\dot{\lambda}_d|$. Typical Cauchy stress $\sigma - \sigma_0^k$ measured during the first cycle (load L_1 and unload U_1) and the last one (load L_{25} and unload U_{25}) are displayed on Fig. 2. Corresponding tangent modulus variations are reported. Representative cases of S_5 and B_3 are illustrated, highlighting important features:

- a mechanical behaviour hysteresis is evidenced between L_1 and U_1. Tangent modulus estimated for S_5 remains nearly constant, with a mean value of 13.8 MPa at L_1, and 14.2 MPa at U_1. It increases (resp. exponentially decreases) up to 2.1 MPa (from 5.6 MPa) for B_3 during L_1 (U_1);
- a cyclic stress relaxation is demonstrated for both samples. Regarding S_5 (B_3), a stress decrease of 256 kPa (125 kPa) is measured at maximal elongation between L_1 and L_{25};
- a residual stretch is measured between L_1 and L_{25}, reaching 0.021 for S_5 against 0.016 for B_3;
- a stabilization of material responses is achieved at L_{25}.

These observations highlight S_i and B_i viscoelastic properties. Their mechanical responses are likely to vary with the applied loading rate.

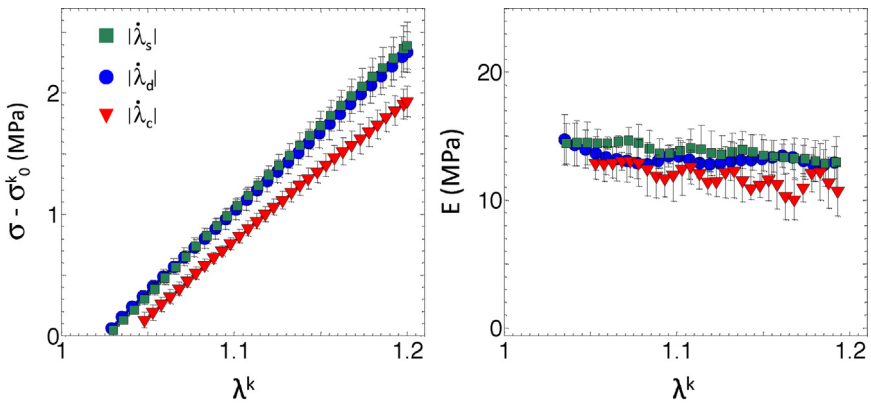

Fig. 3. Comparison between experimental averaged stress $\sigma - \sigma_0^k$ (*left*) and tangent modulus E (*right*) as a function of elongation λ^k during last load L_{25} for synthetic samples S_i ($i \in [1\ldots6]$) tested at loading rate $|\dot{\lambda}^k|$ ($k \in [1\ldots3]$), with $|\dot{\lambda}^1| = |\dot{\lambda}_d| = 4 \times 10^{-2}\,s^{-1}$, $|\dot{\lambda}^2| = |\dot{\lambda}_s| = 1.5 \times 10^{-1}\,s^{-1}$ and $|\dot{\lambda}^3| = |\dot{\lambda}_c| = 1.4 \times 10^{-3}\,s^{-1}$. Error bars correspond to the standard deviations of the measured data.

3.2. Influence of physiological loading rates

3.2.1. Aortic analogue

For each cyclic test k performed at $|\dot{\lambda}^k|$ on S_i, Fig. 3 compares the stress $\sigma - \sigma_0^k$ and tangent modulus E stabilized after L_{25}, in function of λ^k. Data are averaged for S_i, $i \in [1\ldots6]$. Negligible differences are obtained between S_i mechanical responses when tested at $|\dot{\lambda}_d|$ or $|\dot{\lambda}_s|$. Indeed, relative difference obtained on stress–elongation curve comes to 4.7% in average. Discrepancies between E variations are also negligible (average relative difference 4.7%). However, the application of higher physiological elongation rates yields to a stress–hardening effect compared to the response at $|\dot{\lambda}_c|$. The relative difference obtained on stress–elongation curve in cases $k = 1$ and $k = 3$ comes to a mean value of 24.6%, whereas E increases by 9.6% in case $k = 1$. These features are maintained when changing the order of application of the elongation rates (see S_7 and S_8). Therefore, the material stiffening arises from an elongation-rate dependency of its mechanical behaviour. Similar results are obtained when discrimating longitudinal from orthoradial samples, showing Estane isotropic properties (data not shown).

3.2.2. Aortic tissue

Fig. 4 compares the stress–elongation curves obtained after L_1 on B_i, $i \in [3\ldots5]$ at $|\dot{\lambda}_d|$, and on samples B_i, $i \in [1, 2]$ at $|\dot{\lambda}_c|$. Similarly to S_i, the application of the higher physiological elongation rate $|\dot{\lambda}_d|$ yields to a stress–hardening effect regarding to the material response tested at $|\dot{\lambda}_c|$. The relative difference between stress values achieved for both cases comes to 50.2% in average.

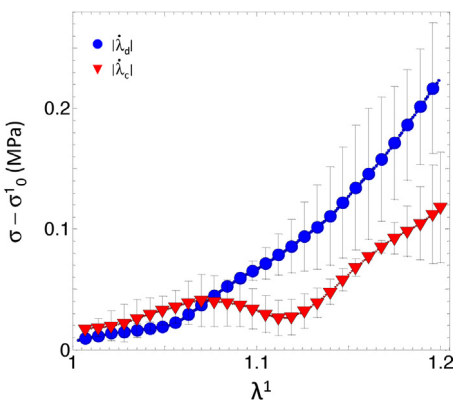

Fig. 4. Comparison between experimental averaged stress $\sigma - \sigma_0^1$ as a function of elongation λ^1 during first load L_1 for biological B_i specimens: B_i, $i \in [3\ldots5]$ are tested at loading rate $|\dot{\lambda}_d|$, while B_i, $i \in [1,2]$ are tested at loading rate $|\dot{\lambda}_c|$. Error bars correspond to the standard deviations of the measured data.

4. Discussion and concluding remarks

This work provides a first attempt to clarify the choice of elongation rate values to prescribe in a tensile testing device when examining the mechanical properties of aortic tissues or analogues. In literature, this choice is commonly set to the lowest allowed value, thereby leaving aside viscoelastic effects. A few previous studies proposed to quantify arterial tissue mechanics with increasing loading velocities [21,20,18] ranging from $\mathcal{O}(10^{-2})\,s^{-1}$ to $\mathcal{O}(10^{2})\,s^{-1}$. Highest velocities tested in [18,21] were representative of those expected in a thoracic impact during automotive collisions. However, the lowest velocities were presented without any connection to clinical measurements existing on arterial dynamics. The present protocol derives from the knowledge of aortic Peterson modulus and the maximum variation of blood pressure. Therefore, given appropriate clinical data [28,29], this approach can adapt as a function of age, gender or pathology, as shown in Table 2.

This protocol has been applied to characterize Estane used to elaborate AA/AAA analogues, and porcine AA, under loading rates experienced by elderly AA tissue. For Estane, negligible differences are obtained when comparing stress–elongation responses between diastolic and systolic elongation rates. However, for both synthetic and biological specimens, results demonstrated a noticeable stiffening of the mechanical response at diastolic rate compared to that obtained under the common rate of $\mathcal{O}(10^{-3})\,s^{-1}$. These findings are supported by investigations by [18] on porcine descending thoracic aorta segments, which demonstrated an increased stiffness with increasing loading rates. In that work, loading rates ranged over four orders of magnitude, from $\mathcal{O}(10^{-2})$ to $\mathcal{O}(10^{1})\,s^{-1}$. Peak elastic modulus increased for the highest loading rates [$\mathcal{O}(10^{0})$ and $\mathcal{O}(10^{1})\,s^{-1}$] compared to the lowest [$\mathcal{O}(10^{-1})$ and

Table 2
Diastolic and systolic elongation rates values corresponding to the present tensile testing procotol as function of age and pathological context. Evaluation according to group-specific average pressure variations and Peterson modulus reported in †[24], ‡[28] and ††[29].

	Age	No	$\lvert\dot{\lambda}_d\rvert$ (s^{-1})	$\lvert\dot{\lambda}_s\rvert$ (s^{-1})
AA	25±2†	10	0.18	0.65
	34±10‡	24	0.13	0.50
	49±3†	8	0.08	0.29
	69±2†	9	0.05	0.19
AAA	70±8.3††	56	0.03	0.12

$\mathcal{O}(10^{-2})\,s^{-1}$]. Yet, similar peak modulus values and stresses were measured for lowest rates, as found in [20] and in present results.

It may be questioned how far Estane remains a suitable candidate to reproduce AA/AAA tissue biomechanics. Once coated into 3D geometries and inflated from diastolic to systolic pressures, [7] showed that realistic levels of wall deformation were measured. The physiological viscoelastic nature of mock AAA motions was further supported by pressure–diameter measurements in a vascular flow simulator [5]. Particularly, the derived E_p value (3.89×10^5 Pa) was comparable to the ones identified from clinical data [29]. However, this study has highlighted important disagreements between its material specificities and that of biological tissue. Research of biomimetic materials is ongoing [30].

This paper focused on the choice of kinematic parameters used in traction tests, a subject of active research [31]. It is shown how to define elongation-rate parameters for tensile testing of AA tissues/analogues, regarding clinical measurements of aortic dilation. To bring the protocol even closer to physiological loadings in future work, a non-zero prestretch of the aorta should be initially considered [32]. Biaxial tensile testing should be performed to produce realistic tensions ratios. Finally, this preliminary study is limited by the low number of collected biological samples, which should be increased to address intersample variability.

Funding

CNRS, Whitaker Scholars program.

Ethical approval

Not required.

Acknowledgements

The authors thank the Surgical Center for Education and Research at Marseille's Nord Hospital (CERC), Pr. S. Berdah and Pr. P. Tropiano for tissue collection. They acknowledge the CNRS and the Whitaker Scholars program for financial support.

Conflict of interest

None declared.

References

[1] Schurink GWH, Aarts NJM, Wilde J, van Baalenn JM, Chuter TAM, Schultze Kool LJ, van Bockel JH. Endoleakage after stent-graft treatment of abdominal aneurysm: implications on pressure and imaging-an in vitro study. J Vasc Surg 1998;28:234–41.
[2] Flora HS, Talei-Faz B, Ansdell L, Chaloner EJ, Sweeny A, Grass A, al. Aneurysm wall stress and tendency to rupture are features of physical wall properties: an experimental study. J Endovasc Ther 2002;9(5):655–75.
[3] Chong CK, How TV. Flow patterns in an endovascular evg for abdominal aortic aneurysm repair. J Biomech 2004;37:89–97.
[4] Gawenda M, Knez P, Winter St, Jaschke G, Wassmer G, Schmitz-Rixen Th, Brunkwall J. Endotension is influenced by wall compliance in a latex aneurysm model. Eur J Vasc Endovasc Surg 2004;27:45–50.
[5] Deplano V, Meyer C, Guivier-Curien C, Bertrand E. New insights into the understanding of flow dynamics in an in vitro model for abdominal aortic aneurysms. Med Eng Phys 2013;35:800–9.
[6] Ene F, Gachon C, Delassus P, Carroll R, Stefanov F, O'Flynn P, Morris L. In vitro evaluation of the effects of intraluminal thrombus on abdominal aortic aneurysm wall dynamics. Med Eng Phys 2011;33:957–66.
[7] Meyer CA, Bertrand E, Boiron O, Deplano V. Stereoscopically observed deformations of a compliant abdominal aortic aneurysm model. J Biomech Eng 2011;133:11004.
[8] Doyle BJ, Cloonan AJ, Walsh MT, Vorp DA, McGloughlin TM. Identification of rupture locations in patient-specific abdominal aortic aneurysms using experimental and computational techniques. J Biomech 2010;43(7):1408–16.
[9] Doyle BJ, Corbett TJ, Cloonan AJ, O'Donnell MR, Walsh MT, Vorp DA, McGloughlin TM. Experimental modelling of aortic aneurysms: novel applications of silicone rubbers. Med Eng Phys 2009;31:1002–12.
[10] Corbett TJ, Doyle BJ, Callanan A, Walsh MT, McGloughlin TM. Engineering silicone rubbers for in vitro studies: creating aaa models and ilt analogues with physiological properties. J Biomech Eng 2010;132(1):011008.
[11] He CM, Roach MR. The composition and mechanical properties of abdominal aortic aneurysms. J Vasc Surg 1994;20:6–13.
[12] Raghavan ML, Webster MW, Vorp DA. Ex vivo biomechanical behavior of abdominal aortic aneurysm: assessment using a new mathematical model. Ann Biomed Eng 1996;24:573–82.
[13] Thubrikar MJ, Labrosse M, Robicsek F, Al-Soudi J, Fowler B. Mechanical properties of abdominal aortic aneurysm wall. J Med Eng Technol 2001;25:133–42.
[14] Holzapfel GA. Determination of material models for arterial walls from uniaxial extension tests and histological structure. J Theor Biol 2006;238:290–302.
[15] Vande Geest JP, Sacks MS, Vorp DA. The effects of aneurysm on the biaxial mechanical behavior of human abdominal aorta. J Biomech 2006;39:1324–34.
[16] Xiong J, Wang SM, Zhou W, Wu JG. Measurement and analysis of ultimate mechanical properties, stress–strain curve fit, and elastic modulus formula of human abdominal aortic aneurysm and nonaneurysmal abdominal aorta. J Vasc Surg 2008;48:189–95.
[17] Sokolis DP, Boudoulas H, Karayannacos PE. Assessment of the aortic stress–strain relation in uniaxial tension. J Biomech 2002;35:1213–23.
[18] Stemper BD, Yoganandan N, Pintar FA. Mechanics of arterial subfailure with increasing loading rate. J Biomech 2007;40:1806–12.
[19] Walraevens J, Willaert B, De Win G, Ranftl A, De Schutter J, Vander Sloten J. Correlation between compression, tensile and tearing tests on healthy and calcified aortic tissues. Med Eng Phys 2008;30:1098–104.
[20] Yang T, Chui CK, Yu RQ, Qin J, Chang SKY. Quasi-linear viscoelastic modeling of arterial wall for surgical simulation. Int J Comput Assist Radiol Surg 2011;6:829–38.
[21] Mohan D, Melvin JW. Failure properties of passive human aortic tissue. i-uniaxial tension tests. J Biomech 1982;15(11):887–93.
[22] Duprey A, Khanafer K, Schlicht M, Avril S, Williams D, Berguer R. In vitro characterisation of physiological and maximum elastic modulus of ascending thoracic aortic aneurysms using uniaxial tensile testing. Eur J Vasc Endovasc Surg 2010;39:700–7.
[23] Deplano V, Knapp Y, Bertrand E, Gaillard E. Flow behaviour in an asymmetric compliant experimental model for abdominal aortic aneurysm. J Biomech 2007;40:2406–13.
[24] Sonesson B, Länne T, Vernersson E, Hansen F. Sex difference in the mechanical properties of the abdominal aorta in human beings. J Vasc Surg 1994;20(6):959–69.
[25] Danpinid A, Luo J, Vappou J, Terdtoon P, Konofagou E. In vivo characterization of the aortic wall stress–strain relationship. Ultrasonics 2010;50:654–65.
[26] Storkholm JH, Frobert O, Gregersen H. Static elastic wall properties of the abdominal porcine aorta *in vitro* and *in vivo*. Eur J Vasc Endovasc Surg 1997;13:31–6.
[27] Schulze-Bauer CAJ, Holzapfel GA. Determination of constitutive equations for human arteries from clinical data. J Biomech 2003;36:165–9.
[28] Long A, Rouet L, Bissery A, Goeau-Brissonniére O, Sapoval M. Aortic compliance in healthy subjects: evaluation of tissue doppler imaging. Ultrasound Med Biol 2004;30(6):753–9.
[29] Long A, Rouet L, Bissery A, Rossignol P, Mouradian D, Sapoval M. Compliance of abdominal aortic aneurysms evaluated by tissue doppler imaging: correlation with aneurysm size. J Vasc Surg 2005;42(1):18–26.
[30] Bailly L, Geindreau C, Orgéas L, Deplano V. Towards a biomimetism of abdominal healthy and aneurysmal arterial tissues. J Mech Behav Biomed Mater 2012;10:151–65.
[31] Cheng S, Clarke EC, Bilston LE. The effects of preconditioning strain on measured tissue properties. J Biomech 2009;42:1360–2.
[32] Han H-C, Fung Y-C. Longitudinal strain of canine and porcine aortas; 1995. Technical Report 5.
[33] Ansarri-Benam A, Legerlotz K, Bader DL, Screen HRC. On the specimen length dependency of tensile mechanical properties in soft tissues: gripping effects and the characteristic decay length. J Biomech 2012;45:2481–2.
[34] Horgan C. End effects in mechanical testing of biomaterials. J Biomech 2013;46:1040–2.